*J. metamorphic Geol.*, 2004, **22,** 495–508 doi:10.1111/j.1525-1314.2004.00530.x

# Calculated phase equilibria for low- and medium-pressure metapelites in the KFMASH and KMnFMASH systems

C. J. WEI[1], R. POWELL[2] AND G. L. CLARKE[3]
[1]*School of Earth and Space Sciences, Peking University, Beijing 100871, China (cjwei@pku.edu.cn)*
[2]*School of Earth Sciences, University of Melbourne, Melbourne, Victoria 3010, Australia*
[3]*School of Geosciences, University of Sydney, Sydney, NSW 2006, Australia*

**ABSTRACT** Petrogenetic grids in the KFMASH and KMnFMASH model systems calculated with the software THERMOCALC 3.1 are presented for the *P–T* range 0.5–12 kbar and 450–900 °C, for assemblages involving garnet, muscovite, chloritoid, biotite, chlorite, staurolite, cordierite, spinel, orthopyroxene, K-feldspar, $Al_2SiO_5$ phases, quartz, water and melt. Based on calculated compatibility diagrams and *P–T* and *T*–$M_{Mn}$ [Mn/(Mg + Fe + Mn)] pseudosections for different metapelitic bulk compositions, the principal conclusions are that the addition of Mn to the KFMASH system: (i) enhances the stability of garnet, and, to a lesser extent, aluminosilicates; (ii) reduces the stability of staurolite, cordierite and, to a lesser extent, chlorite; and (iii) extends the medium pressure stability of muscovite and the low-*P* stability field of K-feldspar. The influence of Mn on individual mineral stabilities is strongly related to rock composition, in particular, to the relative contents of $Al_2O_3$ and $K_2O$. For metapelites of a range of compositions and $M_{Mn}$ values, *P–T* pseudosections in the KFMASH system, in most cases, do not adequately predict the mineral assemblages observed in natural assemblages under medium and low-pressure conditions. In contrast, the *P–T* pseudosections in the KMnFMASH system generally provide more satisfactory results, suggesting that MnO is one of the non-KFMASH components that should not be neglected in documenting the phase equilibria of medium- and low-*P* metapelites.

**Key words:** KFMASH and KMnFMASH systems; phase equilibria; THERMOCALC.

## INTRODUCTION

The model system $K_2O$–FeO–MgO–$Al_2O_3$–$SiO_2$–$H_2O$ (KFMASH) has been studied intensively over recent decades in order to develop petrogenetic grids that account, with various levels of success, for the range of common mineral assemblages in metapelitic rocks. Examples include early qualitative grids based on natural mineral parageneses and experimental data (e.g. Albee, 1965; Hess, 1969; Harte & Hudson, 1979; Labotka, 1981; Pattison & Tracy, 1991; Carrington & Harley, 1995; Droop & Harte, 1995), and later quantitative grids based on internally-consistent thermodynamic data sets (e.g. Spear & Cheney, 1989; Powell & Holland, 1990; Xu *et al*., 1994; Wei & Powell, 2003). In as much as natural rocks are inherently multi-component, a number of studies have been carried out to augment the KFMASH system with additional components such as $Na_2O$, CaO, $TiO_2$, $Fe_2O_3$ and MnO (Mahar *et al*., 1997; Worley & Powell, 1998; White *et al*., 2000, 2001; Tinkham *et al*., 2001).

Given a focus on the ferromagnesian minerals, accompanied by the other main metapelitic minerals that occur in KFMASH, for example muscovite, K-feldspar and the aluminosilicates, the KFMASH system has proved to be a powerful way of systematizing metapelitic mineral equilibria. However, additional components can now be considered and indeed pseudosection calculations can be undertaken in systems such as NCKMnFMASHTO. However, with the above focus, it is still worth considering smaller systems from the point of view of establishing the underlying structure of the bigger systems, particularly via petrogenetic grids. Whereas both $Na_2O$ + CaO and $TiO_2$ + $Fe_2O_3$ are important in understanding the overall mineral equilibria in metapelites, generally they are not critical for understanding the stability of ferromagnesian assemblages. However we argue that MnO is critical, primarily through its role in stabilizing garnet.

MnO is an obvious candidate as an important modifier of KFMASH as Mn substitutes for $Fe^{2+}$ and Mg in ferromagnesian minerals. Mahar *et al*. (1997) calculated a quantitative grid for the KMnFMASH system in the *P–T* range 0–20 kbar and 450–700 °C based on the thermodynamic database of Holland & Powell (1990) to document the effect of Mn on mineral stabilities. Using THERMOCALC 2.7, Tinkham *et al*. (2001) calculated a series of pseudosections for an average biotite-zone metapelite composition from Waterville, Maine, to address the role of variable bulk $Al_2O_3$ and MgO/(FeO + MgO) content on the stability of mineral assemblages in the model system MnNCKFMASH. In addition to not being able to

 

address the stability of plagioclase and zoisite in KFMASH, they concluded that there are significant differences in predicted relationships involving garnet, biotite, staurolite and chloritoid between the two systems. Now, with improvements in the internally-consistent thermodynamic data set, as well as in activity-composition relations for the major silicate phases, it is appropriate to undertake a new calculation of the petrogenetic grid for KMnFMASH for low- and medium-*P* conditions. In this context, there are three purposes for this paper:

(1) to present a petrogenetic grid for KMnFMASH, as well as for the KFMASH system on which it is based, in the *P–T* range 0.5–12 kbar and 450–900 °C for mineral assemblages involving garnet, muscovite, chloritoid, biotite, chlorite, staurolite, cordierite, spinel, orthopyroxene, K-feldspar, aluminosilicate, quartz, $H_2O$ and melt;

(2) to show the effect of Mn on medium- and low-*P* phase equilibria at both subsolidus and suprasolidus conditions using compatibility diagrams;

(3) to illustrate the effect of Mn on the phase equilibria using *P–T* and $T$–$M_{Mn}$ pseudosections in the KFMASH and KMnFMASH systems for representative metapelitic bulk compositions [$M_{Mn}$ is defined by Mn/(Mg + Fe + Mn)].

The calculations were undertaken using THERMOCALC 3.1 (Powell *et al.*, 1998) with the internally-consistent thermodynamic data set of Holland & Powell (1998, and upgrades) and updated models of activity–composition relationships (see the Appendix on the JMG web-site).

## PETROGENETIC GRIDS

### KFMASH grid

The subsystem grids for KFASH and KMASH that provide the framework for the KFMASH grid are presented in Figs S1 & S2, with accompanying notes and information on their invariant equilibria, Table S1. The KFMASH grid is shown in Fig. 1, and the results for the stable invariant equilibria are tabulated in Table S2 (see Supplementary material). There are 13 stable invariant equilibria in the *P–T* range of interest, excluding those with two or three $Al_2SiO_5$ phases. The three muscovite-bearing subsolidus invariant equilibria i1, i2 and i4 are equivalent to the invariant points 9, 8 and 10 of Mahar *et al.* (1997) both in phase combination and topology, but occurring at different *P–T*. The invariant equilibrium equivalent to i1 lies in the andalusite field in the grid of Mahar *et al.* (1997), whereas it is in the kyanite field in Fig. 1, in agreement with the petrologically-favoured conditions of Droop & Harte (1995). The muscovite-absent invariant equilibrium i3 and the univariant reactions emanating from it are important for most metapelites that are insufficiently K-rich, although this point is often neglected when muscovite is assumed to be in excess. The other muscovite-absent invariant equilibrium i5 is metastable with respect to talc and/or orthoamphibole-bearing assemblages. This invariant point and the reactions emanating from it would only be experienced by extremely Mg-rich rocks, of composition inappropriate to the majority of metapelites.

In Fig. 1, reactions 2 (ms + chl + st = bi + als) and 3 (ms + chl + als = bi + cd) do not intersect to form an invariant point, in contrast to the grids of Harte & Hudson (1979); Spear & Cheney (1989); Powell & Holland (1990) and Xu *et al.* (1994). However, it is in agreement with the conclusion of Pattison *et al.* (1999) that the mineral assemblage ms + cd + st + bi (+ q + $H_2O$) is not a stable association (in KFMASH), but a product of polymetamorphism when observed in rocks. Pitra & De Waal (2001) calculated a partial petrogenetic grid in the *P–T* range 0–7 kbar and 500–800 °C in which the sequence of univariant reactions is the same as those labelled 2–10 in Fig. 1.

The suprasolidus part of the KFMASH petrogenetic grid is essentially the same as Fig. 2 of White *et al.* (2001) with two slight differences: (i) the two muscovite dehydration melting reactions 12 and 13 emanate from two KFASH invariant points (fi14 & fi13) with garnet on the low-*T* side in Fig. 1, whereas these two reactions emanate from a KFMASH invariant point with garnet on the high-*T* side in the grid of White *et al.* (2001); and (ii) cordierite-absent univariant reactions that emanate from the four invariant points i7–i10 terminate at four KFASH invariant points fi8–fi11 in Fig. 1, but they form a KFMASH invariant point in the grid of White *et al.* (2001).

Johnson *et al.* (2001) presented calculations in KFMASH that involve a positively-sloped wet solidus in *P–T*, in marked contrast to that in Fig. S1 and in other published studies (i.e. Huang & Wyllie, 1974; LeBreton & Thompson, 1988), as a consequence of using a now-obsolete silicate-melt model outside of its range of applicability.

### KMnFASH, KMnMASH and KMnFMASH grids

The petrogenetic grids for the KMnFMASH system and for the KMnFASH and KMnMASH subsystems are presented in Fig. 2, and calculated results for invariant equilibria in these systems are tabulated in Table S3 (see Supplementary material).

In KMnFASH, there are five invariant equilibria. The two subsolidus ones MnF1 and MnF2 correspond respectively to the two garnet-absent KFASH invariant equilibria fi4 and fi6, displaced to slightly higher *P–T* conditions. The three melt-bearing invariant equilibria MnF3, MnF4 and MnF5 located along the solidus correspond to the three garnet-absent KFASH invariant equilibria fi15, fi10 and fi12, suggesting that addition of Mn has a trivial effect on phase relations at suprasolidus conditions in KMnFASH. In KMnMASH, there are nine invariant equilibria,

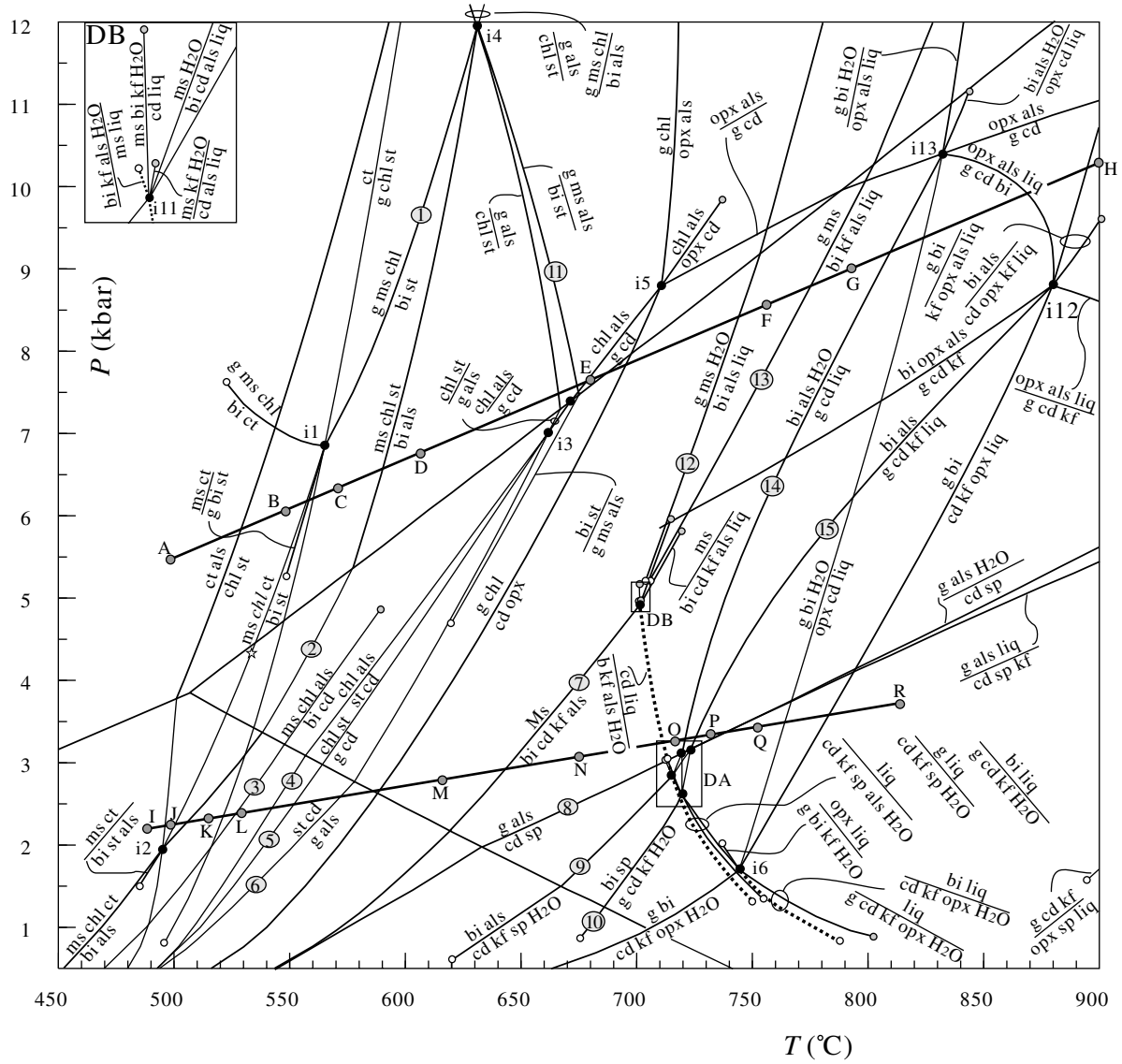


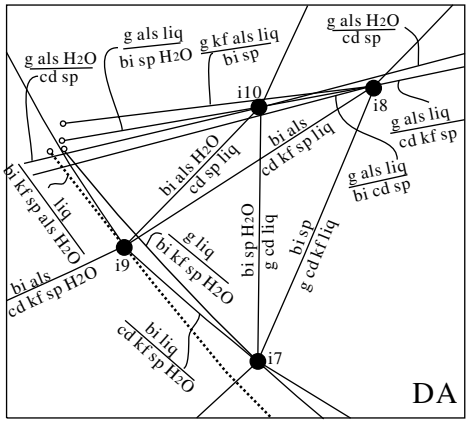


**Fig. 1.** *P–T* projection for the system KFMASH with quartz and $H_2O$ in excess for subsolidus conditions, and for just quartz in excess for suprasolidus conditions. Solid dots with labels i1–i13 refer to the invariant points, and grey-shaded circles with labels 1–15 to the univariant reactions discussed in the text. Heavy dotted lines represent the $H_2O$-saturated solidus in KFMASH. Unfilled stars indicate the location of singularities, and the phases that change sides of the reaction are shown in italics. Smaller open dots refer to the invariant points in KFASH and smaller grey dots to the invariant points in KMASH. Larger grey dots with letters A–R are *P–T* locations of the compatibility diagrams shown in Figs 3 & 4. (DA) shows details around invariant points i7–i10; and (DB) shows details around invariant point i11. Mineral abbreviations: als, $Al_2SiO_5$ phases; bi, biotite; cd, cordierite; chl, chlorite; ct, chloritoid; g, garnet; kf, K-feldspar; liq, melt; ms, muscovite; opx, othopyroxene; q, quartz; st, staurolite; sp, spinel.

corresponding to the nine invariant equilibria in KMASH, each involving the addition of garnet, reflecting a greatly-expanded range of garnet stability with Mn addition. Otherwise the invariant and univariant equilibria in these two subsystems show similar *P–T* conditions and phase topologies.

In the full KMnFMASH system, there are three invariant equilibria. The subsolidus invariant equilibrium Mn1 also occurs in the grid calculated by Mahar *et al.* (1997), at similar *P–T* conditions and with the same phase topology. However, as a result of differences between the KFMASH grids as mentioned above, the slopes of the univariant reactions around Mn1 are different. The two melt-bearing invariant equilibria Mn2 and Mn3 are at almost the same *P–T* conditions as the two garnet-absent invariant equilibria i9 and i11 in the KFMASH grid. In addition to these three invariant equilibria, there are six independent univariant reactions emanating from KFMASH and KMnMASH invariant points. As shown in Fig. 2, the univariant reactions in KMnFMASH mostly follow the equivalent KFMASH garnet-absent reactions, substantially expanding the stability range of garnet.

## COMPATIBILITY DIAGRAMS

To show the dependence of mineral assemblage and the compositions of co-existing minerals on *P–T* and bulk composition, a series of MnFM and AFM compatibility diagrams were calculated for two traverses marked on Figs S1 & S2 and Figs 1 & 2. The MnFM compatibility diagrams are projected from muscovite, aluminosilicate, quartz and $H_2O$ onto MnO–FeO–MgO; the AFM compatibility diagrams from muscovite, garnet, quartz and $H_2O$. Suprasolidus projection is from silicate melt rather than $H_2O$, and from K-feldspar rather than muscovite once muscovite + quartz has broken down.

The compatibility diagrams for the first traverse, from A to H, approximately along a 25 °C $km^{-1}$ geotherm representing medium-pressure metamorphism, are shown in Fig. 3. In Fig. 3a, both chlorite and biotite are complete solid solutions between the Fe- and Mg-end members. In Al-rich rocks chl–ct–ky may occur, as shown in the AFM diagram, coexisting with Mn-rich garnet as shown in the MnFM diagram. As *P–T* increases, the KMnFASH reaction, g + ms + chl = bi + ct, leads to the breakdown of Fe-rich chlorite, giving the bi-ct-chl divariant triangle in Fe-rich compositions, and the KMnFASH reaction, ct + als = g + st, produces staurolite in Al-rich rocks. The ct–ky tie line is replaced by chl–st through the full system reaction, ct + als = g + chl + st. At this stage, Fe-rich garnet becomes stable through the KFASH reaction, bi + fct = alm + ms. This garnet is shown as a hollow bar in Fig. 3b to signify that the phases coexisting with this garnet are Mn-free. With *P–T* increase to cross the full system reaction, ct + ms = g + chl + bi + st, chloritoid disappears and the st–bi tie line becomes stable, Fig. 3c. The KFMASH reaction, ct + ms = g + bi + st, produces the divariant assemblage g–bi–st. When the KMnFMASH reaction, chl + st + ms = g + bi + als, is crossed, the chl–st tie line gives way to ky–bi in the AFM diagram and g-bi in the MnFM, Fig. 3d. As *P–T* increases from D, the changes in phase topology are mainly controlled by the subsystem reactions. At E, the KMnMASH reaction ms + chl = g + bi + als has led to the disappearance of Mg-chlorite, and the KFASH reaction fst = alm + als and KFMASH reaction bi + st = g + als result in the breakdown of staurolite, Fig. 3e. At F, melting has commenced in $H_2O$-saturated rocks, and the KFASH reaction, ms + bi = kf + alm + liq, has led to the decomposition of Fe-rich biotite, Fig. 3f. Across the KMnMASH reaction g + ms = kf + bi + als + liq, muscovite breaks down and K-feldspar coexists with aluminosilicate. In Fe-rich rocks, the KFASH reaction, bi = kf + opx + alm + liq, produces a divariant triangle g–bi–opx, Fig. 3g. Across the KFMASH reaction, g + bi = kf + opx + als + liq, orthopyroxene can co-exist with aluminosilicate, Fig. 3h.

For a traverse from I to R, approximately along a 60 °C $km^{-1}$ geotherm representing low-pressure metamorphism, the changes in phase topology are shown in Fig. 4. In Fig. 4i, the chl–ct tie line is present and Fe-chlorite has broken down through the KMnFASH subsystem reaction, g + ms + chl = bi + ct. As *P–T* increases to cross the KMnFASH reaction ct + als = g + st, staurolite is formed in Fe–Al-rich compositions, Fig. 4j. From J to K, the full system reactions ms + chl + ct = g + bi + als and ms + ct = g + bi + st + als lead to the coexistence of biotite and aluminosilicate, the disappearance of chloritoid in Fe-rich rocks, and the KMnMASH reaction g + chl + als = cd produces cordierite in Mg-rich rocks, Fig. 4k. With *P–T* increase to meet the full system reaction g + ms + chl + als = bi + cd, the chl–g or chl–and tie lines give way to bi–cd, and the KMnFASH reaction ms + st = g + bi + als results in the disappearance of staurolite, Fig. 4l. At M, the KMnMASH reactions g + ms + chl = bi + cd and g + ms + bi = cd + kf result in the disappearance, respectively, of magnesian chlorite and biotite, Fig. 4m. Across the reaction g + ms = bi + cd + kf + als, muscovite breaks down and K-feldspar coexists with aluminosilicate, Fig. 4n. Across the solidus, melt appears in the full system and the subsystems, but otherwise the phase topologies are similar to those at N. The

**Fig. 2.** *P–T* projection for the system KMnFMASH and the subsystems KMnFASH and KMnMASH with quartz and $H_2O$ in excess for subsolidus conditions, and quartz for suprasolidus conditions. Invariant points: solid squares with labels Mn1–Mn3 for the KMnFMASH, open squares with labels MnF1–MnF5 for the KMnFASH, grey shaded squares with labels MnM1–MnM9 for the KMnMASH, the solid dots for the KFMASH, the smaller open dots for the KFASH and the smaller grey shaded dots for the KMASH. Univariant lines: heavy solid lines for the KMnFMASH, doted lines for the KMnFASH, and dashed lines for the KMnMASH. Larger grey dots with letters A–R are *P–T* locations of the compatibility diagrams shown in Figs 3 & 4. Box DA shows details around invariant point Mn2; and DB shows details around invariant point Mn3. For mineral abbreviations see Fig. 1.

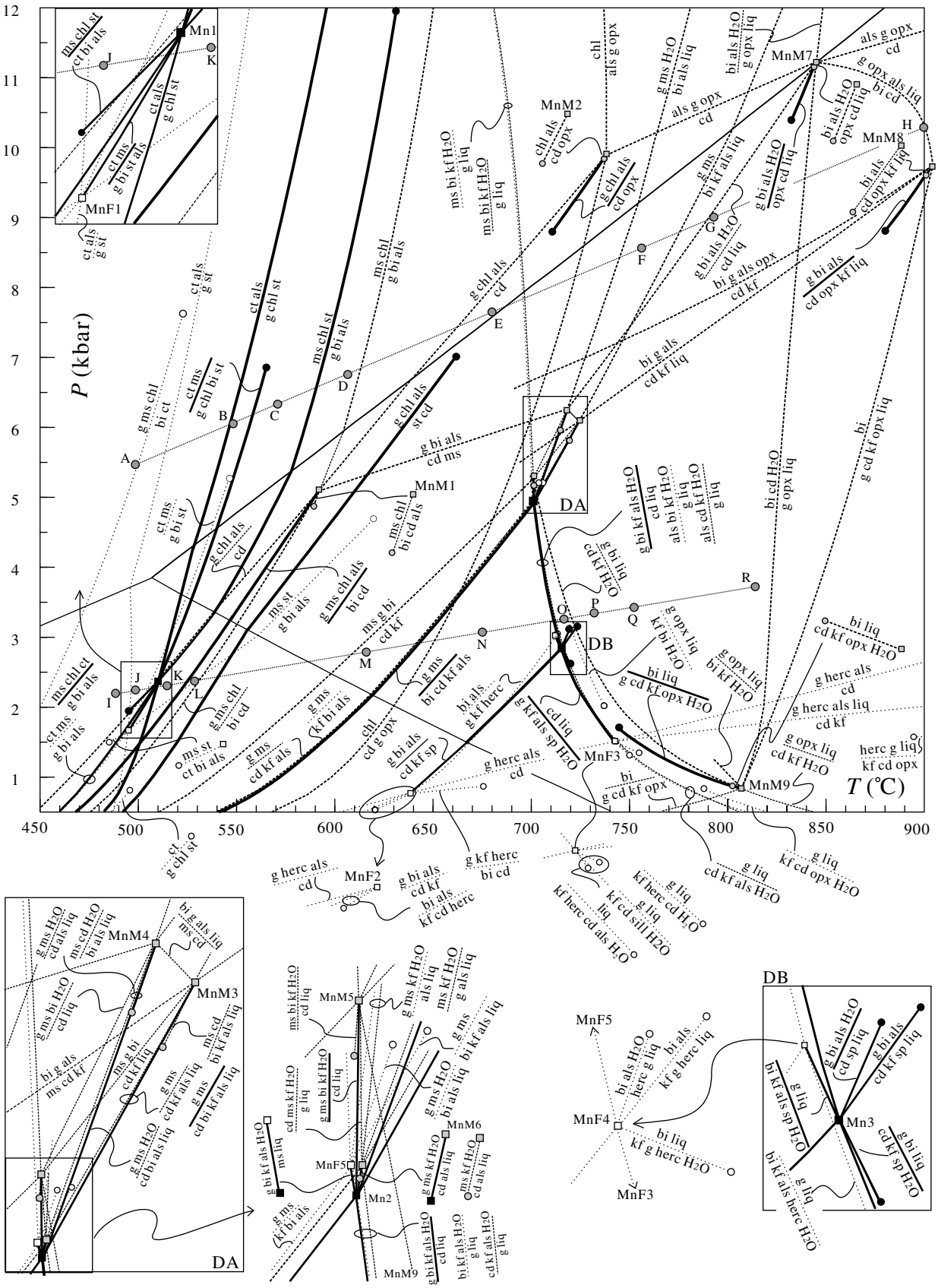

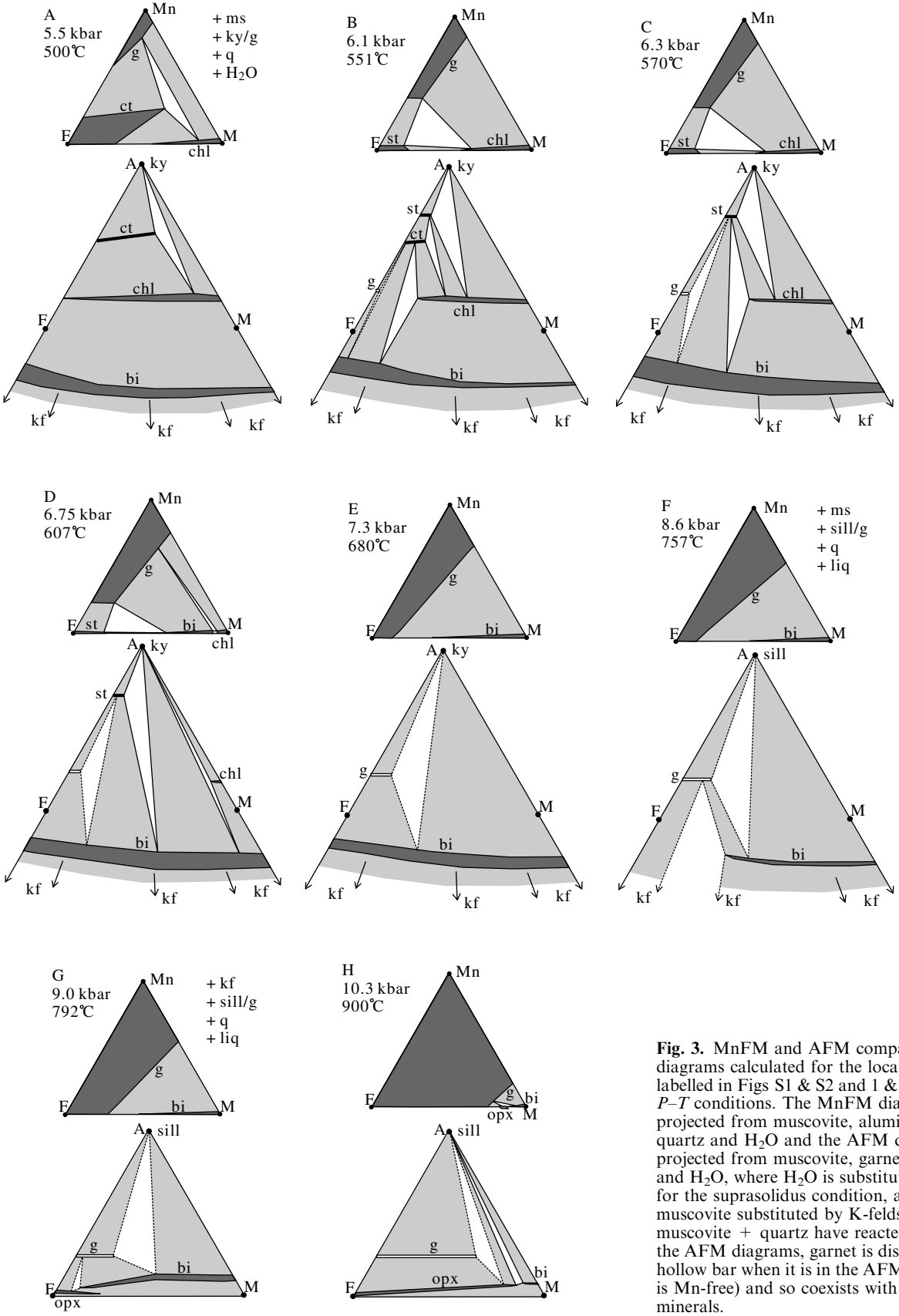


**Fig. 3.** MnFM and AFM compatibility diagrams calculated for the locations A–H labelled in Figs S1 & S2 and 1 & 2 and their *P–T* conditions. The MnFM diagrams are projected from muscovite, aluminosilicate, quartz and $H_2O$ and the AFM diagrams projected from muscovite, garnet, quartz and $H_2O$, where $H_2O$ is substituted by melt for the suprasolidus condition, and the muscovite substituted by K-feldspar when muscovite + quartz have reacted out. In the AFM diagrams, garnet is displayed as a hollow bar when it is in the AFM plane (i.e. is Mn-free) and so coexists with Mn-free minerals.

KFASH reaction als + bi = kf + alm + liq produces a divariant triangle g–bi–sill in KFMASH, Fig. 4o. Now the KFMASH reaction bi + als = g + cd + kf + liq leads to the bi–sill tie line being replaced by g–cd, Fig. 4p. The KFASH reaction alm + als = herc and the KFMASH reaction g + als + liq = cd + sp + kf result in the appearance of spinel in Fe–Al-rich rocks, while in Fe-rich rocks, the KFASH reaction bi = kf + opx + alm + liq leads to the breakdown of Fe-biotite and the appearance of orthopyroxene, Fig. 4q. Across the KFMASH reaction g + bi = kf + opx + als + liq, the g–bi tie line is replaced by opx–cd in Al–poor rocks, Fig. 4r.

## PSEUDOSECTIONS

Phase relations are best illustrated and understood using pseudosections, where a bulk composition is incorporated into calculations based on the grids. The pseudosections constructed below involve quartz and $H_2O$ in excess for subsolidus conditions; for suprasolidus conditions, quartz is in excess and $H_2O$ sufficient to just saturate the mineral assemblage immediately subsolidus at medium pressure is included (White *et al.*, 2001). The bulk compositions are given in terms of $H_2O$:$Al_2O_3$:MgO:FeO:$K_2O$:MnO, on a mole basis, appropriate for suprasolidus conditions, with the corresponding KFMASH composition involving the omission of the MnO. For subsolidus conditions, this amount of $H_2O$ is replaced by that sufficient to saturate the mineral assemblage. Three bulk compositions were selected for the pseudosections presented below, representing a range of relative $Al_2O_3$, $K_2O$ and MnO contents.

### A typical pelite composition used by Mahar *et al.* (1997)

The typical pelite composition used by Mahar *et al.* (1997) is similar to the average composition of the Scottish Dalradian pelites calculated by Atherton & Brotherton (1982), and to the low-Al pelites proposed by Spear (1993). After modifying the aluminium contents by removing albite and anorthite from the composition, this typical pelite composition has $H_2O$:$Al_2O_3$:MgO:FeO:$K_2O$:MnO = 20.02:30.74:17.35:21.60:10.01:0.29. KFMASH and KMnFMASH *P–T* pseudosections are presented for this bulk composition in Fig. 5a,b. The KFMASH pseudosection is dominated by di- and trivariant fields with a few quadrivariant fields in the high-*P*/*T* and high-*T* parts of the diagram. There is one invariant point (i4), and segments of 11 univariant reactions that are encountered by this bulk composition. The KMnFMASH pseudosection (Fig. 5b) is dominated by tri- and quadrivariant fields with a few divariant and quinivariant fields. There is only one segment of a univariant reaction that is 'seen' by the bulk composition.

From a comparison of Fig. 5a,b, the expected observation is that garnet-bearing assemblages are stable over a much larger area of *P–T* space in the Mn-bearing pelite, especially for subsolidus conditions. For example, garnet is confined to $P > 8$ kbar at $T > 580$–$590$ °C in Fig. 5a, whereas in Fig. 5b, garnet stability is extended to $P > 3$–$4$ kbar for $T > 520$–$540$ °C. However, the phase relations in low-*P* fields ($P < 3$–$4$ kbar) and at suprasolidus conditions are similar in the two pseudosections.

For a *P–T* array typical of Barrovian-type metamorphism as indicated by path A in Fig. 5a, b (Spear, 1993), the KFMASH pseudosection would predict a sequence of mineral assemblages: ms + chl + bi → ms + chl + bi + st → ms + bi + st → ms + bi + st + ky → ms + bi + ky → ms + bi + sill (+ q + $H_2O$). However this does not match the sequence observed in the Barrovian zones. The same *P–T* array on the KMnFMASH grid predicts the metamorphic grade sequence: ms + chl + bi → g + ms + chl + bi → g + ms + chl + bi + st → g + ms + bi + st → g + ms + bi + st + ky → g + ms + bi + ky → g + ms + bi + sill (+q+$H_2O$), closely matching the observed Barrovian grade sequence of biotite, garnet, staurolite, kyanite and sillimanite zones. This implies that the KFMASH grid is not sufficient to elucidate phase relations of common medium-*P* metapelites, which contain even small amounts of MnO. Figure 5b shows that the index minerals staurolite and kyanite form across KMnFMASH divariant fields that correspond to the KFMASH univariant reactions 1 and 11.

A *P–T* array appropriate to typical low-*P* metamorphism is path B in Fig. 5a,b. The metamorphic grade sequence is: ms + chl + bi → ms + chl + bi + and → ms + bi + and → ms + bi + and + cd → ms + bi + cd → ms + bi + cd + kf → bi + cd + kf (+ q + $H_2O$). This is similar to the metapelitic facies series 2a of Pattison & Tracy (1991) and Pattison *et al.* (1999), except that the assemblages above the breakdown of muscovite contain sillimanite in facies series 2a. A metamorphic process dominated by isobaric heating at conditions of $P \approx 1$ kbar would result in the metamorphic sequence: ms + chl + bi → ms + chl + bi + cd → ms + bi + cd → ms + bi + cd + kf → bi + cd + kf (+ q + $H_2O$), corresponding to the metapelitic facies series 1a of Pattison & Tracy (1991) and Pattison *et al.* (1999). If the isobaric heating occurred at $P = 3$–$4$ kbar, staurolite and sillimanite instead of cordierite and andalusite occur, in agreement with the metapelitic facies series 3 of Pattison & Tracy (1991) and Pattison *et al.* (1999). For these low-*P* types of metamorphism, both Fig. 5a,b predict similar mineral assemblages.

The suprasolidus part of Fig. 5a is almost the same as fig. 3 in White *et al.* (2001) because of the similarity in both the base petrogenetic grid and the chosen bulk composition. These phase relations are governed mainly by the muscovite and biotite dehydration-melting reactions (12–15), as also documented by Spear *et al.* (1999). From a comparison of Fig. 5b with

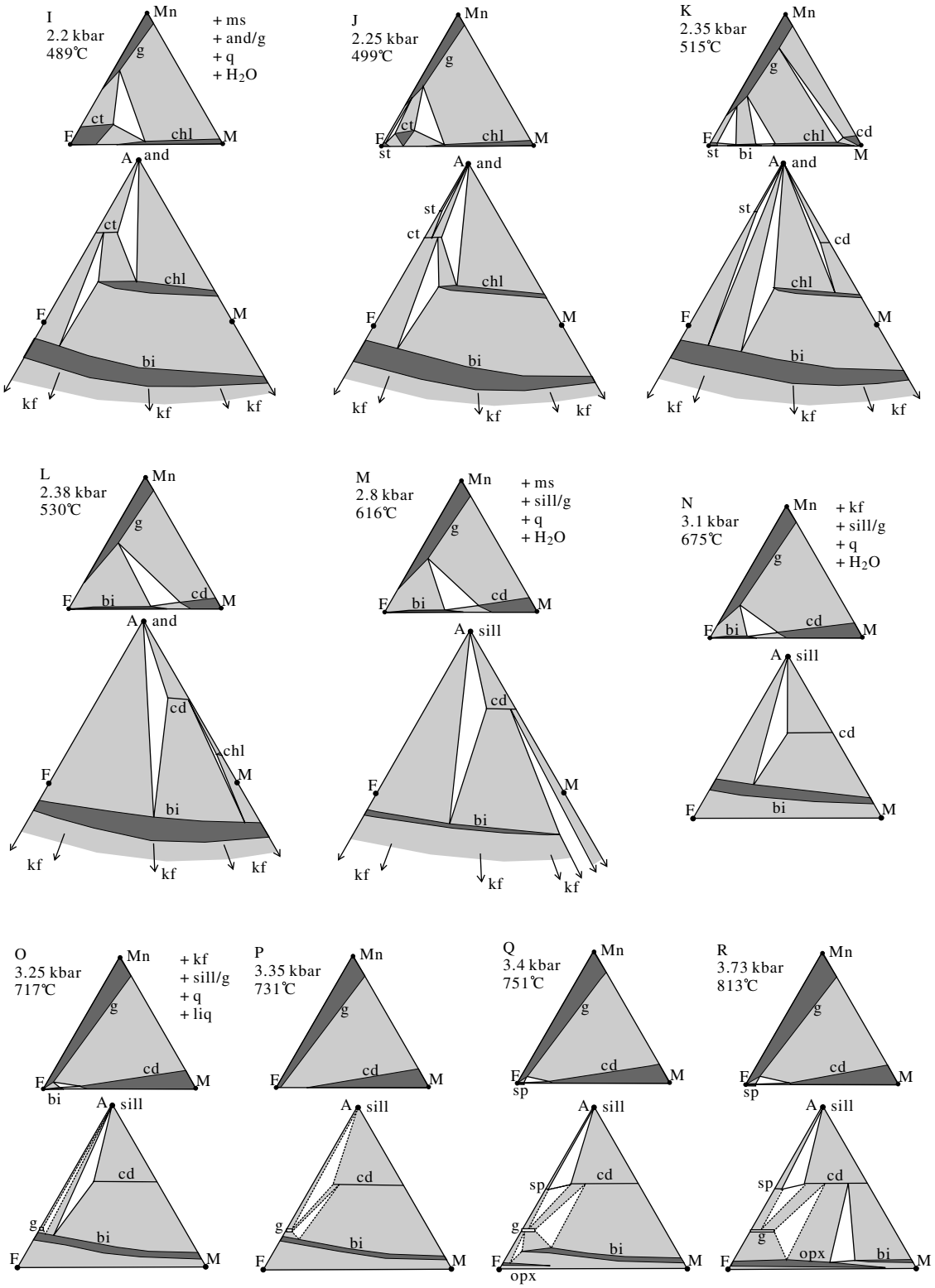


**Fig. 4.** MnFM and AFM compatibility diagrams calculated for the locations I–R labelled in Figs S1 & S2 and 1 & 2 and their *P–T* conditions. The MnFM diagrams are projected from muscovite, aluminosilicate, quartz and $H_2O$ and the AFM diagrams projected from muscovite, garnet, quartz and $H_2O$, where $H_2O$ is substituted by melt for the suprasolidus condition, and muscovite substituted by K-feldspar when muscovite is out. In the AFM diagrams, garnet is displayed as a hollow bar when it is in the AFM plane (i.e. is Mn-free) and so coexists with Mn-free minerals.

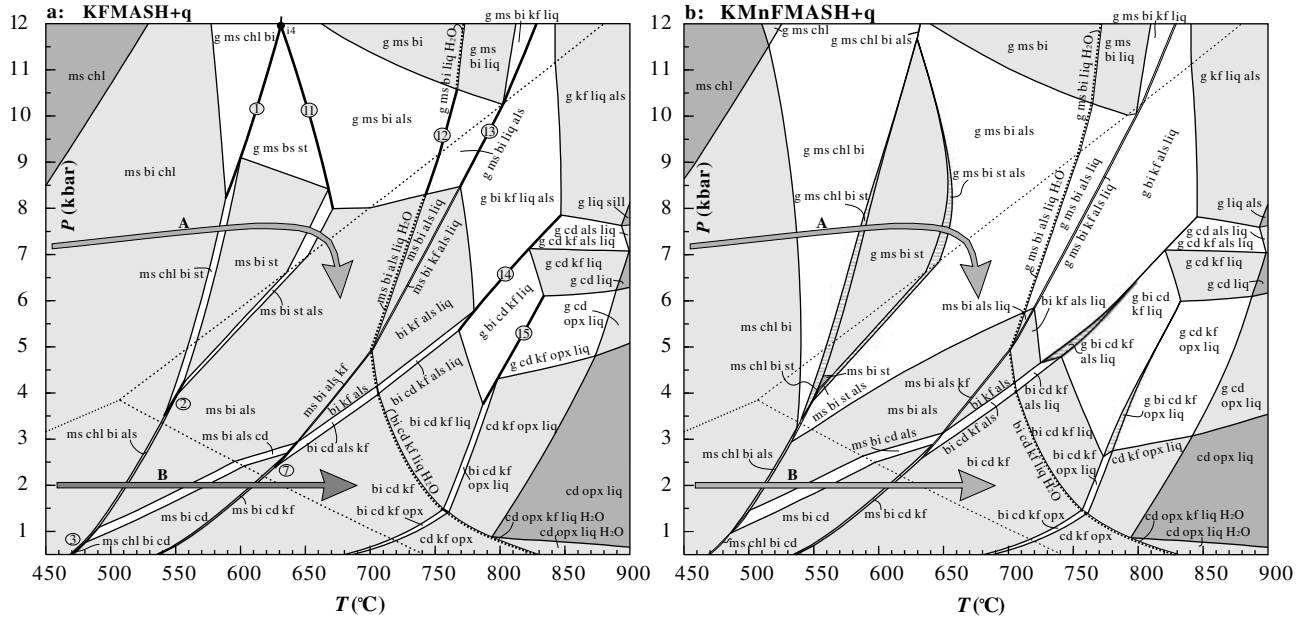


**Fig. 5.** KFMASH (a) and KMnFMASH (b) *P–T* pseudosections for a typical pelite used by Mahar *et al.* (1997) (see text). The pseudosections show the invariant points (solid dots), univariant reactions (heavy solid lines) some of which with number in grey-shaded circle are corresponding to those in Fig. 1, and divariant fields (unshaded), trivariant fields (lighter-grey shaded) and quadrivariant fields (darker-grey shaded) in the KFMASH (a), and divariant fields (filled with horizontal lines), trivariant fields (unshaded), quadrivariant fields (lighter-grey shaded) and quinivariant fields (darker-grey shaded) in the KMnFMASH (b). Heavy dotted lines represent the $H_2O$-saturated solidus. Paths A and B represent the *P–T* arrays characteristic of medium-*P* and low-*P* metamorphism, respectively.

Fig. 5a, it is clear that adding Mn into the KFMASH system does not lead to a significant change in the suprasolidus phase relations except for expanding garnet stability to lower *P* and *T* conditions.

To further illustrate the effect of Mn on phase relations, $T$–$M_{Mn}$ pseudosections were drawn for $P =$ 7 and 2 kbar (Fig. 6a,b) for this bulk composition. The incoming of garnet is dependent on the $M_{Mn}$ in the bulk composition: for $M_{Mn} > 0.023$ at medium pressure and $M_{Mn} > 0.032$ at low pressure, garnet will be present throughout the temperature range being considered. In addition, as $M_{Mn}$ increases, the width of the staurolite stability field is reduced slightly.

### A migmatic gneiss from the Altay orogenic belt, Xinjiang, China

The Altay orogenic belt was formed by a late Palaeozoic collision between the Siberian and Junggar plates (Windley *et al.*, 2002). This belt exposes low-*P* type metamorphism with biotite, garnet, staurolite, andalusite, sillimanite, and migmatite zones (Zhuang, 1994). From the migmatite zone, a representative sample (A152) consists of garnet (12 vol.%), biotite (12%), cordierite (10%), K-feldspar (5%), sillimanite (3%), plagioclase (15%) and quartz (40%) with a small amount of ilmenite, graphite and apatite. Representative microprobe analyses of the main minerals in weight per cent in the order ($SiO_2$, $Al_2O_3$, FeO, MnO, MgO, CaO, $K_2O$) are: garnet (38.20, 22.21, 26.73, 7.21, 5.40, 0.94, 0.0); biotite (35.62, 19.32, 15.39, 0.09, 11.12, 0.0, 9.77); and cordierite (48.47, 32.35, 5.36, 0.36, 9.53, 0.0, 0.0). From these modes and compositions, the bulk composition were calculated as $H_2O$:$Al_2O_3$: MgO:FeO:$K_2O$:MnO = 15.60:28.15:20.18:26.56:5.11: 4.41. In generating this composition, all of the garnet modes were used as the garnet grains are not chemically zoned. Using this composition, KFMASH and KMnFMASH *P–T* pseudosections were calculated (Fig. 7a,b). The KFMASH pseudosection in Fig. 7a contains mainly trivariant fields and a few divariant and quadrivariant fields. There is only one invariant point (i4) and segments of 15 univariant reactions that are 'seen' by the bulk composition. The KMnFMASH pseudosection in Fig. 7b is dominated by tri- and quadrivariant fields with two quinivariant fields at high-*T* conditions. The subsolidus parts of these two pseudosections are significantly different: garnet stability is enlarged to encompass the entire *P–T* range of interest, the stability fields of staurolite and chlorite at medium pressures ($P > 4$ kbar) is reduced, and the field of muscovite enlarged. At low-*P* conditions, the stability fields of chlorite and orthopyroxene are appreciably reduced. The suprasolidus parts of Fig. 7a,b are similar, implying that Mn has little effect on the suprasolidus phase relations.

For sample A152, the effect of Mn on the mineral stability can also be seen in the $T$–$M_{Mn}$ pseudosections

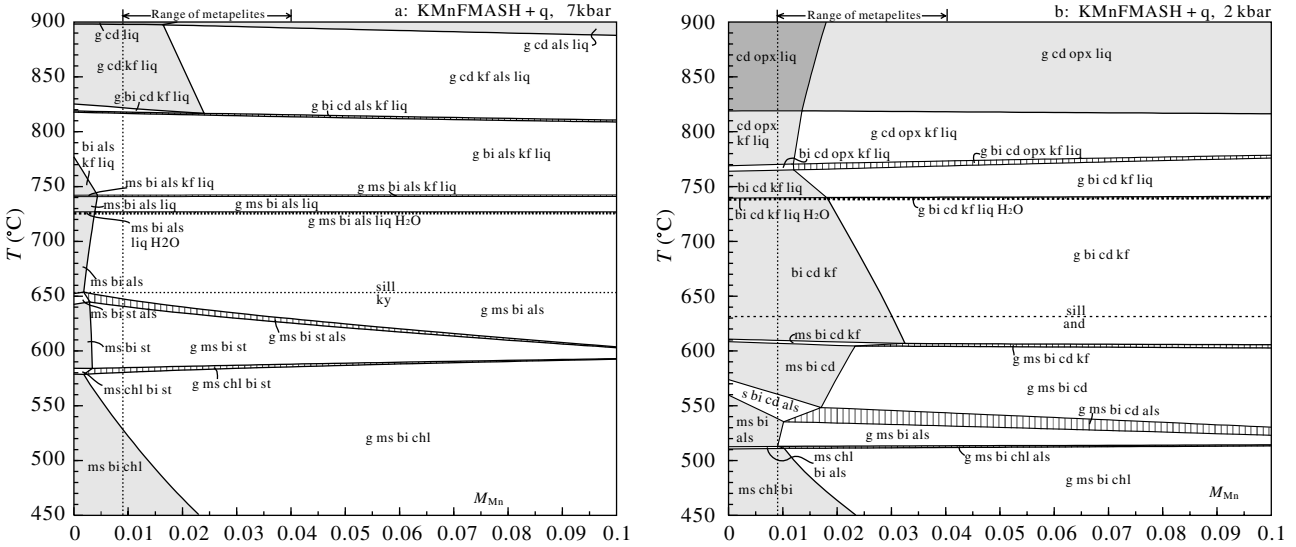


**Fig. 6.** $T$–$M_{Mn}$ pseudosections in the KMnFMASH system calculated at 7 kbar (a) and 2 kbar (b) for the typical pelite used by Mahar *et al.* (1997) with a range of $M_{Mn} = 0$–0.1, showing divariant fields (filled with vertical lines), trivariant fields (unshaded), quadrivariant fields (lighter-grey shaded) and quinivariant fields (darker-grey shaded). Heavy dotted lines represent the $H_2O$-saturated solidus. The range of $M_{Mn}$ for metapelites is from Symmes & Ferry (1992). The vertical dashed line represents the $M_{Mn}$ of the typical pelite used by Mahar *et al.* (1997).

in Fig. 8a,b. At medium-pressure conditions, as represented in Fig. 8a, the sequence of mineral assemblages for the normal metapelite with $M_{Mn} =$ 0.008–0.04 is similar to the mineral assemblage sequence in KFMASH ($M_{Mn} = 0$ in Fig. 8a) except that garnet stability expands with $M_{Mn}$ for $T < 600$ °C. When $M_{Mn} < 0.05$, the upper limit of the staurolite stability field slides subtly to lower $T$ as $M_{Mn}$ is increased, but for $M_{Mn} > 0.05$ staurolite stability is dramatically reduced. The stability fields of the $Al_2SiO_5$ phases are expanded with increasing $M_{Mn}$. In addition, cordierite stability at suprasolidus conditions is decreased for $M_{Mn} > 0.035$.

## A garnet mica schist from the Altay orogenic belt, Xinjiang, China

A garnet mica schist (sample A91) from the garnet zone of the Altay low-pressure metamorphic belts, Xinjiang, China, is composed of garnet (10 vol.%), biotite (25%), muscovite (5%), plagioclase (50%) and quartz (8%) with a small amount of ilmenite, graphite and apatite. Representative microprobe analyses of the main minerals in weight per cent in the order ($SiO_2$, $Al_2O_3$, FeO, MnO, MgO, CaO, $K_2O$) are: garnet rim (37.36, 21.12, 26.79, 10.81, 2.67, 1.46, 0.0); biotite (35.95, 18.52, 18.27, 0.17, 11.24, 0.0, 9.31); and muscovite (47.50, 32.73, 1.71, 0.0, 1.32, 0.0, 10.03). With these modes and compositions, the bulk composition were calculated as $H_2O$:$Al_2O_3$:MgO:FeO:$K_2O$:MnO = 18.13:20.48:21.77:27.62:8.87:3.13. Only half of the garnet mode was used as the garnet is chemically zoned (e.g. Carson *et al.*, 1999). Using this bulk composition, KFMASH and KMnFMASH $P$–$T$ pseudosections were calculated (Fig. 9a,b). The KFMASH pseudosection in Fig. 9a is dominated by trivariant fields with some quadrivariant and divariant fields. There are small segments of nine univariant reactions 'seen' by the bulk composition. The KMnFMASH pseudosection (Fig. 9b) is dominated by quadrivariant fields with some tri- and divariant fields and with only a small segment of a univariant reaction encountered by the bulk composition. The two pseudosections are clearly different. At medium pressures ($P > 3$–4 kbar), the KFMASH pseudosection has extensive fields that include staurolite and aluminosilicate. In the KMnFMASH pseudosection (Fig. 9b), staurolite and aluminosilicate are not stable. In addition, the complicated mineral assemblage fields (about 20) at medium pressure conditions in the subsolidus part of Fig. 9a are reduced to only four in Fig. 9b. The changes in mineral assemblages at medium pressure conditions from the KFMASH to KMnFMASH systems are clearly displayed in Fig. 10a. For rocks with $M_{Mn} < 0.02$, the mineral assemblages in the two systems are similar, except that garnet stability is expanded for higher $M_{Mn}$ for $T < 600$ °C. However, for rocks with $M_{Mn} >$ 0.02–0.03, the mineral assemblages in the Mn-bearing system are quite different from those in KFMASH; the muscovite stability field enlarges dramatically, and staurolite and aluminosilicate are not stable. For medium pressure conditions, the $H_2O$-saturated solidus and the appearance of K-feldspar slide to lower $T$ conditions with increasing $M_{Mn}$. However, the suprasolidus assemblages at $T > 800$ °C are not strongly influenced by $M_{Mn}$ content.

In Fig. 10b, the $H_2O$-saturated solidus and most mineral assemblages above the solidus do not show

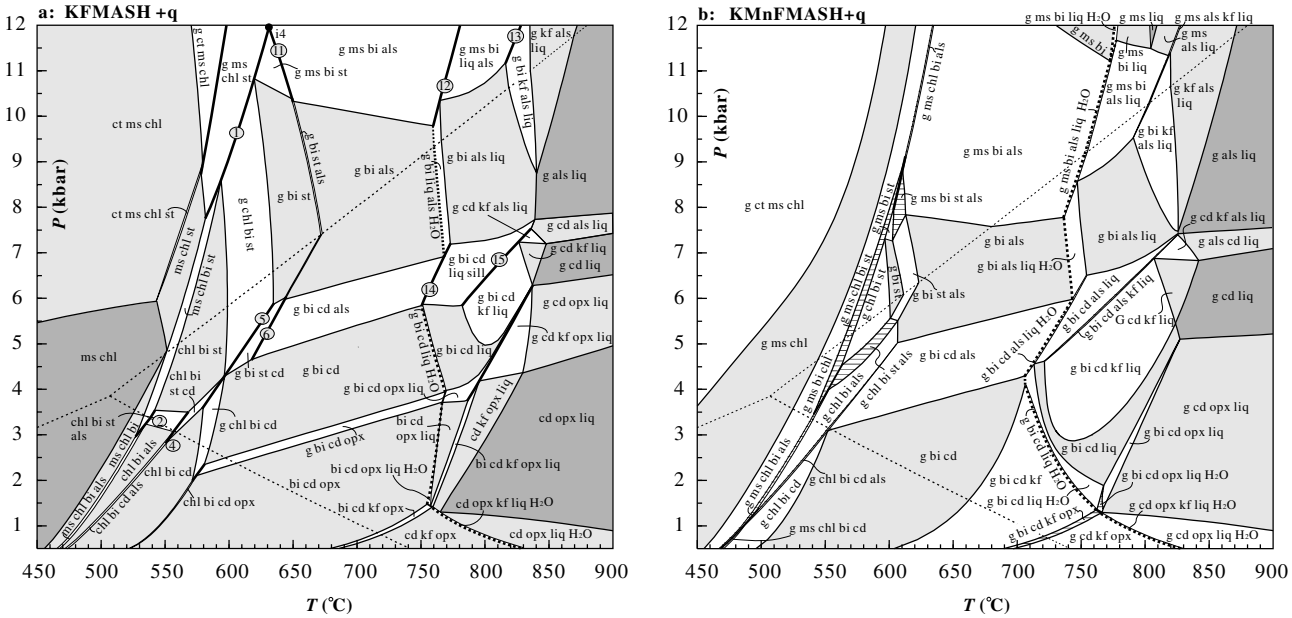


**Fig. 7.** KFMASH (a) and KMnFMASH (b) $P$–$T$ pseudosections for a migmatic gneiss sample A152 (see text). For field ornaments see Fig. 5.

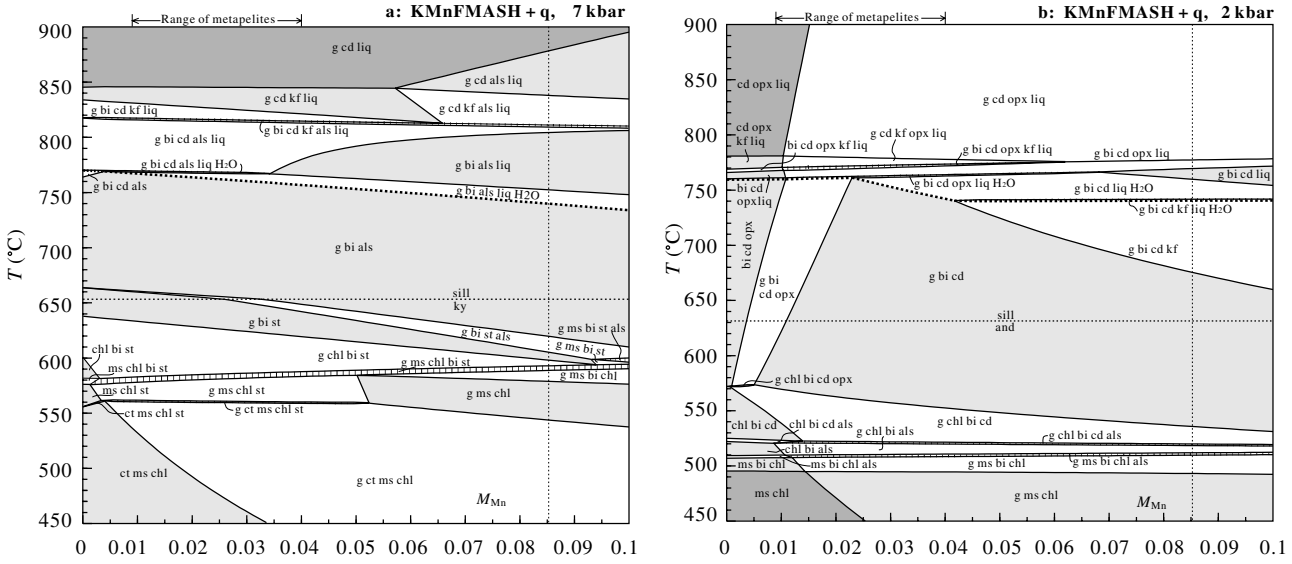


**Fig. 8.** $T$–$M_{Mn}$ pseudosections in the KMnFMASH system calculated at 7 kbar (a) and 2 kbar (b) for the migmatic gneiss sample A152 with a range of $M_{Mn} = 0$–0.1. The vertical dashed line represents the $M_{Mn}$ content of sample A152. For field ornaments see Fig. 6.

any pronounced control by $M_{Mn}$ content. In the subsolidus part of Fig. 10b, KMnFMASH with $M_{Mn} < 0.065$ has similar assemblages (but plus garnet) to KFMASH ($M_{Mn} = 0$). However, cordierite is not stable for $M_{Mn} > 0.065$. Muscovite-out and cordierite-in (when present) are not influenced by $M_{Mn}$, but chlorite-out and K-feldspar-in slide to lower $T$ as $M_{Mn}$ increases.

The observed mineral assemblage g + bi + ms (+ q + $H_2O$) is trivariant in KFMASH and stable for $P > 8.5$ kbar and $T > 600$ °C in the pseudosection shown in Fig. 9a. In the KMnFMASH pseudosection (Fig. 9b), this assemblage is quadrivariant and stable for $P > 4.5$ kbar and $T > 550$ °C. On the basis of conventional geothermobarometry, Zhuang (1994) estimated temperature conditions between 500 and 570 °C for this

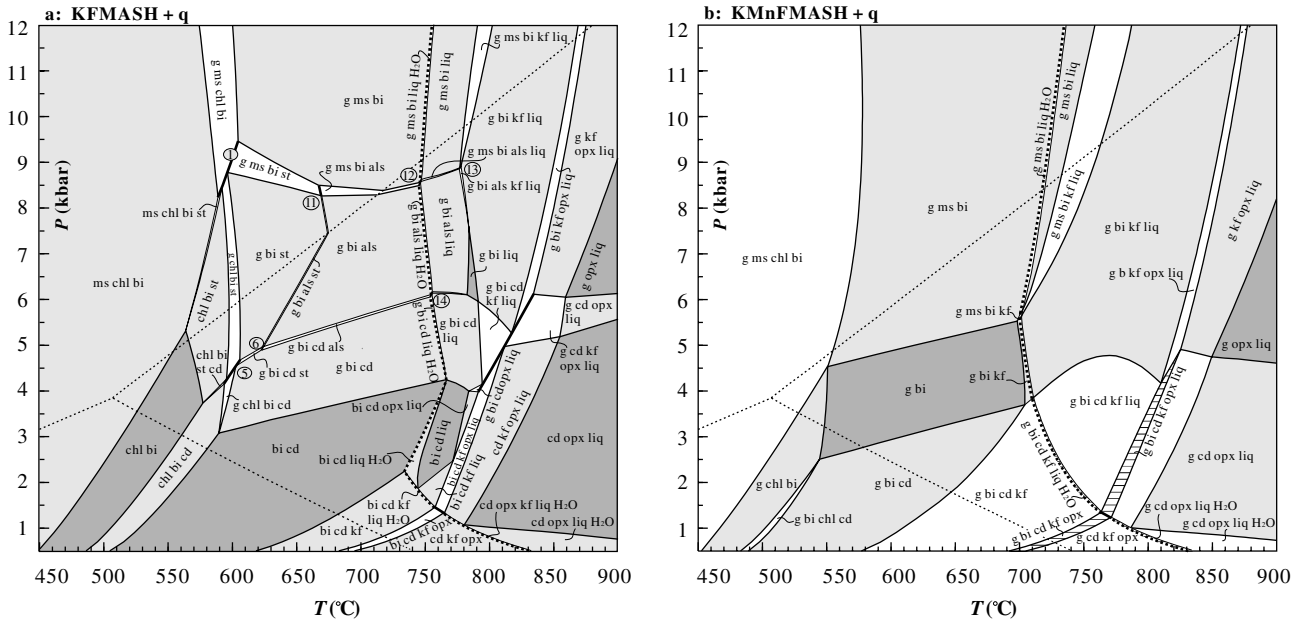


**Fig. 9.** KFMASH (a) and KMnFMASH (b) *P–T* pseudosections for a garnet mica schist sample A091 (see text). For field ornaments see Fig. 5.

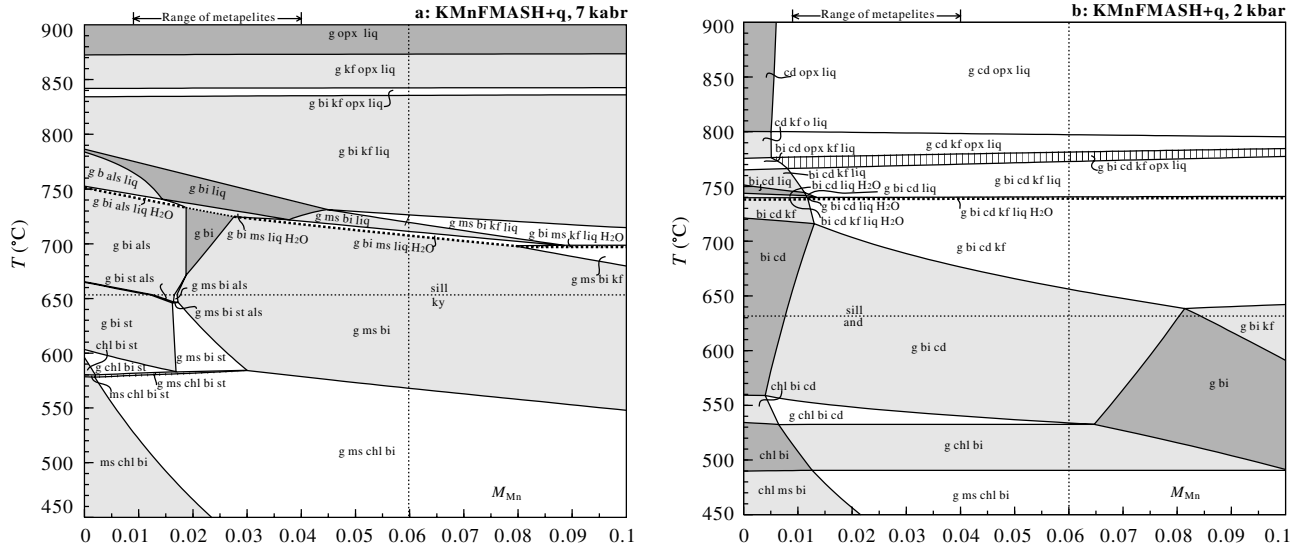


**Fig. 10.** *T*–$M_{Mn}$ pseudosections in the KMnFMASH system calculated at 7 kbar (a) and 2 kbar (b), for the garnet mica schist sample A091 for a range of $M_{Mn} = 0$–0.1. The vertical dashed line represents the $M_{Mn}$ of sample A091. For field ornaments see Fig. 6.

garnet zone, and a pressure range of 3.5–5.0 kbar for the adjacent andalusite zone. Only the phase relations in the KMnFMASH are consistent with these petrological deductions.

## CONCLUSIONS

Our petrogenetic grid in KMnFMASH is more consistent with petrological observations than previously published grids (Spear & Cheney, 1989; Powell & Holland, 1990; Xu *et al.*, 1994; Mahar *et al.*, 1997; Johnson *et al.*, 2001). Together with the calculated compatibility diagrams and pseudosections, these petrogenetic grids are powerful in delineating the phase equilibria of medium- and low-pressure metapelites.

The effect of Mn on mineral stability in metapelites has been documented in several studies, all emphasizing that the partitioning of Mn into garnet stabilizes garnet-bearing assemblages (e.g. Spear & Cheney, 1989; Symmes & Ferry, 1992; Mahar *et al.*, 1997;

Tinkham *et al.*, 2001). Based on the calculated *equilibria*, this conclusion is confirmed and added to:
(i) The addition of Mn into the KFMASH system does clearly enhance the stability of garnet as recognized in previous work: it is stable over the whole *P–T* range of interest for $M_{Mn} > 0.025$–0.03.
(ii) The expansion of garnet stability fields leads to different effects on the stabilities of other phases. Generally, as $M_{Mn}$ increases, the stability fields of staurolite, cordierite and, to a lesser extent, of chlorite reduce. The stability fields of the $Al_2SiO_5$ phases and, at medium pressure, of muscovite as well as K-feldspar at low pressure are extended.
(iii) The effect of Mn on mineral stabilities is strongly related to bulk composition, in particular, to the relative contents of $Al_2O_3$ and $K_2O$. For example, the three bulk compositions discussed above have restricted $X_{Fe} = 0.55$–0.58, but different relative contents of $Al_2O_3$ and $K_2O$. For an AFM diagram representing lower amphibolite facies, the typical subaluminous pelite used by Mahar *et al.* (1997) plots below the garnet–chlorite tie line. Sample A152, which is comparatively poor in $K_2O$, plots just above the garnet–chlorite tie line. Sample A091, being comparatively poor in $Al_2O_3$, projects below the FM border. For the bulk compositions close to the typical pelite used by Mahar *et al.* (1997), Mn mostly affects subsolidus phase relations at medium pressure; it is less important for subsolidus phase relations at low pressure and for suprasolidus phase equilibria. For bulk compositions comparatively rich in $Al_2O_3$ but poor in $K_2O$ (sample A152), Mn affects the subsolidus phase equilibria at both medium and low pressures, and has trivial effects at suprasolidus conditions. For bulk compositions comparatively rich in $K_2O$ but poor in $Al_2O_3$ (sample A091), Mn affects all subsolidus phase equilibria and most of the suprasolidus equilibria.

For metapelites with various compositions and $M_{Mn}$ values, *P–T* pseudosections in the KFMASH system, in most cases, cannot match natural assemblages in rocks of medium- and low-pressure. In comparison, *P–T* pseudosections in the KMnFMASH system can generally provide satisfactory results, for example, for typical subaluminous pelite bulk composition predicting the sequence of isograds and assemblages observed in Barrow's zones. These observations suggest that, among the non-KFMASH components, MnO is the one element that should not be neglected in documenting the phase equilibria of medium- and low-*P* metapelites.

## ACKNOWLEDGEMENTS

This work was financially supported by the National Natural Science Foundation of China (grant number: 40172031) and undertaken while CJW was a visitor in the School of Geosciences at the University of Sydney. We are most grateful to M. Guiraud and G. Rebay for helpful reviews of the manuscript. D. Robinson is thanked for his careful editorial work.

## SUPPLEMENTARY MATERIAL

The following material is available from http://www.blackwellpublishing.com/products/journals/suppmat/JMG/JMG530/JMG530sm.htm

**Fig. S1.** *P–T* projection for the subsystem KFASH.

**Fig. S2.** *P–T* projection for the subsystem KMASH.

**Table S1.** Calculated results for invariant equilibria in KFASH and KMASH subsystems.

**Table S2.** Calculated results for invariant equilibria KFMASH subsystem.

**Table S3.** Calculated results for invariant equilibria in KMnFASH, KMnMASH and KMnFMASH systems.

## Appendix

Notes on KFASH grid.

Mixing models, mineral and end member formulae and composition variables.

THERMOCALC data file.

## REFERENCES

Albee, A. L., 1965. A petrogenetic grid for the Fe–Mg silicates of pelitic schists. *American Journal of Science*, **263,** 512–536.

Atherton, M. P. & Brotherton, M. S., 1982. Major element composition of the pelite of Scottish Dalradian. *Geological Journal*, **17,** 185–221.

Carrington, D. P. & Harley, S. L., 1995. Partial melting and phase relations in high-grad metapelites: an experimental petrogenetic grid in the KFMASH system. *Contributions to Mineralogy and Petrology*, **120,** 270–291.

Carson, C. J., Powell, R. & Clarke, G. L., 1999. Calculated mineral equilibria for eclogites in $CaO–Na_2O–FeO–MgO–Al_2O_3–SiO_2–H_2O$: application to the Pouèbo Terrane, Pam Peninsula, New Caledonia. *Journal of Metamorphic Geology*, **17,** 9–24.

Droop, G. T. R. & Harte, B., 1995. The effect of Mn on the phase relations of medium-grade pelites: constraints from natural assemblages on petrogenetic grid topology. *Journal of Petrology*, **36,** 1549–1578.

Harte, B. & Hudson, N. F. C., 1979. Pelitic facies series and the temperatures and pressure of Dalradian metamorphism in eastern Scotland. In: *The Caledonides of the British Isles reviewed*, Special publication, 8. (eds Harris, A. L., Holland, C. H. & Leake, B. E.), pp. 323–337. Geological society of London, London.

Hess, P. C., 1969. The metamorphic paragenesis of cordierite in pelitic rocks. *Contributions to Mineralogy and Petrology*, **24,** 191–207.

Holland, T. J. B. & Powell, R., 1990. An enlarged and updated internally consistent thermodynamic dataset with uncertainties and correlations:the system $K_2O–Na_2O–CaO–MgO–MnO–FeO–Fe_2O_3–Al_2O_3–TiO_2–SiO_2–C–H_2–O_2$. *Journal of Metamorphic Geology*, **8,** 89–124.

Holland, T. J. B. & Powell, R., 1998. An internally consistent thermodynamic data set for phases of petrological interest. *Journal of Metamorphic Geology*, **16,** 309–343.

Huang, W. L. & Wyllie, P. J., 1974. Melting reactions of muscovite with quartz and sanidine in the $K_2O–Al_2O_3–SiO_2–H_2O$ system to 30 kilobars and an outline of paragonite meting reactions. *American Journal of Science*, **274,** 378–395.

Johnson, T. E., Hudson, N. F. C. & Droop, G. T. R., 2001. Partial melting in the Inzie Head gneisses: the role of water and a petrogenetic grid in KFMASH applicable to anatectic pelitic migmatites. *Journal of Metamorphic Geology*, **19,** 99–118.

Labotka, T. C., 1981. Petrology of an andalusite-type regional metamorphic terrane, Panamint Mountains, California. *Journal of Petrology*, **22,** 261–296.

LeBreton, N. & Thompson, A. B., 1988. Fluid-absent (dehydration) melting of biotite in metapelites in the early stages of crustal anatexis. *Contributions to Mineralogy and Petrology*, **99,** 226–237.

Mahar, E. M., Baker, J. M., Powell, R., Holland, T. J. B., Howell, N., 1997. The effect of Mn on mineral stability in metapelites. *Journal of Metamorphic Geology*, **15,** 223–238.

Pattison, D. R. M. & Tracy, R. J., 1991. Phase equilibria and thermobarometry of metapelites. In: *Contact Metamorphism. Reviews in Mineralogy*. (ed. Kerrick, D. M.), Vol. 26, pp. 105–206. Mineral Society of America, Washington, DC.

Pattison, D. R. M., Spear, F. S. & Cheney, J. T., 1999. Polymetamorphic origin of muscovite + cordierite + staurolite + biotite assemblages: implications for the metapelitic petrogenetic grid and for *P–T* paths. *Journal of Metamorphic Geology*, **17,** 685–703.

Pitra, P. & De Waal, S. A., 2001. High-temperature, low-pressure metamorphism and development of prograde symplectites, Marble Hall Fragment, Bushveld Complex (south Africa). *Journal of Metamorphic Geology*, **19,** 311–325.

Powell, R. & Holland, T. J. B., 1990. Calculated mineral equilibria in the pelite system KFMASH ($K_2O$–FeO–MgO–$Al_2O_3$–$SiO_2$–$H_2O$). *American Mineralogist*, **75,** 367–380.

Powell, R., Holland, T. J. B. & Worley, B., 1998. Calculating phase diagrams involving solid solutions via non-linear equations, with examples using Thermocalc. *Journal of Metamorphic Geology*, **16,** 577–588.

Spear, F. S., 1993. *Metamorphic Phase Equilibrium and Pressure–Temperature–Time Paths*, pp. 337–391. Mineralogical Society of America, Washington, DC.

Spear, F. S. & Cheney, J. T., 1989. A petrogenetic grid for pelitic schists in the system $SiO_2$–$Al_2O_3$–FeO–MgO–$K_2O$–$H_2O$. *Contributions to Mineralogy and Petrology*, **101,** 149–164.

Spear, F. S., Kohn, M. J. & Cheney, J. T., 1999. *P–T* paths from anatectic pelites. *Contributions to Mineralogy and Petrology*, **134,** 17–32.

Symmes, G. H. & Ferry, J. M., 1992. The effect of whole-rock Mn-content on the stability of garnet in pelite schists during metamorphism. *Journal of Metamorphic Geology*, **10,** 221–237.

Tinkham, D. K., Zuluaga, C. A. & Stowell, H. H., 2001. Metapelite phase equilibria modeling in MnNCKFMASH: the effect of variable $Al_2O_3$ and MgO/(MgO + FeO) on mineral stability. *Geological Materials Research*, **3,** 1–42.

Wei, C. J. & Powell, R., 2003. Phase relations in high-pressure metapelites in the system KFMASH ($K_2O$–FeO–MgO–$Al_2O_3$–$SiO_2$–$H_2O$) with application to natural rocks. *Contributions to Mineralogy and Petrology*, **145,** 301–315.

White, R. W., Powell, R., Holland, T. J. B. & Worley, B., 2000. The effect of $TiO_2$ and $Fe_2O_3$ on metapelitic assemblages at greenschist and amphibolite facies conditions: mineral equilibria calculations in the system $K_2O$–FeO–MgO–$Al_2O_3$–$SiO_2$–$H_2O$–$TiO_2$–$Fe_2O_3$. *Journal of Metamorphic Geology*, **18,** 497–511.

White, R. W., Powell, R. & Holland, T. J. B., 2001. Calculation of partial melting equilibria in the system $Na_2O$–CaO–$K_2O$–FeO–MgO–$Al_2O_3$–$SiO_2$–$H_2O$ (NCKFMASH). *Journal of Metamorphic Geology*, **19,** 139–153.

Windley, B. F., Kröner, A., Guo, J. H., Qu, G. S., Li, Y. Y. & Zhang, C., 2002. Neoproterozoic to Paleozoic geology of the Altai Orogen, NW China: new zircon age data and tectonic evolution. *The Journal of Geology*, **110,** 719–737.

Worley, B. & Powell, R., 1998. Singularities in NCKFMASH ($Na_2O$–CaO–$K_2O$–FeO–MgO–$Al_2O_3$–$SiO_2$–$H_2O$). *Journal of Metamorphic Geology*, **16,** 169–188.

Xu, G. W., Will, T. M. & Powell, R., 1994. A calculated petrogenetic grid for the system $K_2O$–FeO–MgO–$Al_2O_3$–$SiO_2$–$H_2O$, with particular reference to contact–metamorphosed pelites. *Journal of Metamorphic Geology*, **12,** 99–119.

Zhuang, Y. X., 1994. *Tectonothermal evolution in space and time and orogenic process of Altaide, China*. 402p. Jilin Scientific and Technical Press, Changchun, China. (In Chinese with English abstract).

*Received 20 October 2003; revision accepted 4 April 2004.*